Cleavage of an aromatic ring and radical migration

Journal:	*Faraday Discussions*
Manuscript ID	FD-ART-01-2022-000012.R1
Article Type:	Paper
Date Submitted by the Author:	15-Feb-2022
Complete List of Authors:	Mebel, Alexander; Florida International University, Chemistry and Biochemistry Frenklach, Michael; University of California at Berkeley, Department of Mechanical Engineering

SCHOLARONE™
Manuscripts

Cleavage of an aromatic ring and radical migration

Alexander M. Mebel[a,*] and Michael Frenklach[b,*]

[a]Department of Chemistry and Biochemistry, Florida International University, Miami, Florida, 33199, USA. E-mail: mebela@fiu.edu

[b]Department of Mechanical Engineering, University of California at Berkeley, Berkeley, California, 94720-1740, USA. E-mail: frenklach@berkeley.edu

Abstract

The present study undertakes a theoretical evaluation of thermal decomposition of aromatic-ring radicals. Potential energy surfaces and associated reaction rate coefficients were calculated for 1- and 2-naphthalenyl, acetanaphthylenyl, and pyrenyl radicals. Kinetic Monte-Carlo simulations were performed to examine the rates of ring cleavage in two sooting laminar premixed flames of ethylene. The simulations showed that the thermal aromatic-ring cleavage is comparable in rate to oxyradical decomposition in a heavier-sooting flame. The simulation also revealed, unexpectedly, fast internal ring radical migration, comparable in frequency to reaction events of aromatic growth.

1. Introduction

Detailed understanding of aromatic-ring growth is of interest to many fields, including combustion, atmospheric chemistry, astrophysics, and synthesis of carbonaceous materials, like carbon black, carbon nanotubes, and recently graphene. Unravelling the complexity of aromatic structures and their transformations has been aided by increasing sophistication of experimental approaches to sampling and authentication of molecular intermediates. At the same time, quantum chemistry and reaction-rate theory have become reliable theoretical tools in exploration of various reaction pathways and quantification of their kinetics and thermodynamics. Recent application of these tools uncovered a variety of chemical reaction pathways of aromatic-ring growth and oxidation in combustion and astrophysical environments. The focus of the present study is on a "silent" feature of these aromatic mechanisms, thermal decomposition or cleavage of aromatic-ring radicals. Such processes impact evolution of aromatics in two (related) aspects.

First, aromatic-ring radicals are intermediates in aromatics growth and their thermal decomposition constitutes the reverse of the growth. In fact, the growth steps are highly reversible reactions and overcoming their reversibility, especially for one- to four-ring aromatics, is the essence of the current understanding and kinetic modeling of the process.[1,2] The second aspect of thermal decomposition of aromatic-ring radicals is their important role in destruction of aromatic structure during oxidation[3] and growth.[4]

In light of their significance, we undertake in the present study theoretical evaluation of thermal decomposition of several structurally foundational aromatic-ring radicals, such as naphthalenyl, acetanaphthylenyl, and pyrenyl. We re-examine decomposition reactions of two-ring aromatics and extend the analysis to include additional reaction channels and additional three- and four-ring aromatic systems.

2. Computational Methods

Geometry optimizations of the reactants, intermediates, transition states, and products of the isomerization and decomposition reactions of the $C_{10}H_7$ (naphthalenyl), $C_{12}H_7$ (acetanaphthylenyl), and $C_{16}H_9$ (pyrenyl) radicals were performed within the density functional theory (DFT) B3LYP method with the 6-311G(d,p) basis set,[5,6] with vibrational frequencies and zero vibrational energy (ZPE) corrections computed at the same level of theory. The DFT calculations utilized the Gaussian 09 software package.[7] Single-point energies of optimized structures were rectified employing the G3(MP2,CC) model chemistry scheme,[8-10] which uses the coupled clusters CCSD(T)/6-311G(d,p)

energy with a correction for a more complete G3Large basis obtained at the Møller-Plessett second-order perturbation theory MP2 level:

$$E[G3(MP2,CC)] = E[CCSD(T)/6\text{-}311G(d,p)] + E[MP2/G3Large)] - E[MP2/6\text{-}311G(d,p)] +$$
$$+ ZPE[B3LYP/6\text{-}311G(d,p)]$$

The G3(MP2,CC) calculations were carried out employing the MOLPRO 2010 program.[11]

The calculated energetic and molecular parameters, such as vibrational frequencies and rotational constants, were used to compute rate constants of the isomerization and decomposition reactions in a wide range of pressures and temperatures, including those typical for sooting flame conditions, by solving the Rice-Ramsperger-Kassel-Marcus kinetic Master Equation (RRKM-ME)[12] within the framework of the Rigid-Rotor, Harmonic-Oscillator (RRHO) model. The MESS code[13] was utilized in the RRKM-ME calculations. The collisional energy transfer in RRKM-ME was described by using the "exponential decay" model,[14] where the temperature dependence of the parameter α for the deactivating energy transfer function is expressed as $\alpha(T) = \alpha_{300} (T/300)^n$. For naphthalenyl radicals we used the reaction scheme and the potential energy surface (PES) reported earlier in the study of the kinetics of the $C_6H_4C_2H + C_2H_2$ reaction[15] extended by including additional ring cleavage channels found in the present work. In particular, Lennard-Jones parameters ε and σ for $C_{10}H_7$ adopted from that work were 390 cm^{-1} and 4.46 Å, respectively, with $\alpha_{300} = 424$ cm^{-1} and $n = 0.62$. The same collisional parameters were also utilized for the slightly larger acetanaphthylenyl $C_{12}H_7$ system. For pyrenyl, we used Lennard-Jones parameters proposed by Wang and Frenklach for pyrene,[16] $\varepsilon = 834.9$ cm^{-1} and $\sigma = 7.24$ Å, in conjunction with the parameters for the bath gas N_2 taken from Vishnyakov et al. ($\varepsilon = 101.5$ cm^{-1} and $\sigma = 3.62$ Å).[17,18] For uniformity, we kept the same $\alpha_{300} = 424$ cm^{-1} and $n = 0.62$ values for pyrenyl, but it is our experience that for the reactions involving PAH, differences in pressure-dependent rate constants using these values and with the "universal" values for hydrocarbons proposed by Jasper and Miller,[19] $\alpha_{300} = 247$ cm^{-1} and $n = 0.85$, do not exceed 10%.[20]

The Electronic Supporting Information (ESI) for this paper includes a table listing calculated rate constants at different pressures (Table S1) and input files for RRKM-ME calculations using the MESS package, which incorporate optimized Cartesian coordinates of all relevant stationary structures on the $C_{12}H_7$ and $C_{16}H_9$ PESs, their relative energies, and vibrational frequencies.

3. Results and Discussion
3.1. Potential energy surfaces
3.1.1. Naphthalenyl radicals

The PES for isomerization and unimolecular decomposition of 1- and 2-naphthalenyl radicals is illustrated in Figure 1. The majority of the considered pathways have been studied in the earlier works[15,21] in relation to the reaction of the 1-ethynylphenyl radical $C_6H_4C_2H$ with acetylene C_2H_2 but here we included some additional ring cleavage channels. The 2-naphthalenyl radical **n2** is 0.2 kcal/mol lower in energy than 1-naphthalenyl **n1** and represents the global minimum on the $C_{10}H_7$ surface. **n1** and **n2** can rearrange to one another by a 1,2-H shift via a barrier of 60.2 kcal/mol relative to **n2**. β-Scissions of C-H bonds in the radicals can produce aryne species, 1,2- and 2,3-didehydronaphthalenes (**n-p3** and **n-p4**) from 2-naphthalenyl and only 1,2-didehydronaphthalene from 1-naphthalenyl. The β-C-H bond energies in **n1** and **n2** lie in the range of 77-80 kcal/mol, which is close to the corresponding C-H bond energy in C_6H_5, 79.7 kcal/mol.[22] Similar to the phenyl radical,[23-25] the H elimination reactions from 1- and 2-naphthalenyls are predicted to have no exit barriers. In addition to the H loss, the radicals can undergo a C-C bond β-scission, which results in a cleavage of one of the aromatic rings. In particular, such β-scission in **n1** leads to the intermediate **n3** lying 53.1 kcal/mol higher in energy than **n1** via a barrier of 59.4 kcal/mol. Next, **n3** can be also subjected to either C-H or C-C bond β-scission. The former leads to the 1,2-diethynylbenzene + H product (**n-p2**) and latter produces $C_6H_4C_2H$, the 1-ethynylphenyl radical, plus acetylene (**n-p1**). These unimolecular decomposition pathways are computed to be 84.9 and 94.6 kcal/mol endothermic and to feature exit barriers of 91.9 and 97.7 kcal/mol, respectively, all relative to **n1**. Thus, the ring cleavage decomposition pathways of 1-naphthalenyl are significantly less favorable than the H elimination producing 1,2-didehydronaphthalene. The ring cleavage processes in **n2** is even less competitive. The β-scission of the C-C bond in **n2** adjacent to the second aromatic ring produces intermediate **n4** which features a CHCHCCH side chain linked to the C_6H_4 ring. The barrier for this reaction step is 60.2 kcal/mol and **n4** resides 53.9 kcal/mol higher in energy than 2-naphthalenyl. Next, **n4** can undergo a relatively facile 1,5-H migration from the terminal C atom in the side chain to the ring via a barrier of 34.4 kcal/mol forming **n5**, 79.9 kcal/mol above **n2**. Intermediate **n5** can give rise to the C_6H_5 + diacetylene C_4H_2 product (**n-p5**) via a two- or three-step pathways. In the two-step route, **n5** first rearranges to **n6** by 1,3-hydrogen migration in the side chain and then splits the C_4H_2 moiety. In the three-step path, **n5** first features a 1,2-H shift accompanied with a three-member closure in the side chain leading to **n7** and then the ring reopens forming **n6**. The two-step pathway is favored in terms of the highest barrier, 118.0 kcal/mol relative to **n2**, as compared to 121.7 kcal/mol for the three-step pathway. The C_6H_5 + C_4H_2 product resides 92.9 kcal/mol higher in energy than 2-naphthalenyl, which is comparable with the energy of the $C_6H_4C_2H$ + C_2H_2 product, 94.8 kcal/mol.

4

Another C-C bond β-scission in **n2** can in principle occur between two CH groups neighboring to the radical position forming the intermediate **n8** with two side chains, CH and CHCCH on the aromatic ring, via a barrier of 77.6 kcal/mol. However, **n8** is expected to be metastable because the barrier in the reverse direction is only 0.5 kcal/mol. Possible decomposition of the **n4** intermediate by simple cleavage of the C-C bond between the ring and the side chain will not be competitive since the *o*-benzyne + *n*-C_4H_3 product in this case is evaluated to lie ~147 kcal/mol higher in energy than **n2**.[22,26] Clearly, for 2-naphthalenyl, isomerization to 1-naphthalenyl via H migration and H losses forming didehydronaphthalenes represent the most favorable isomerization and decomposition channels and the direct ring cleavage is not likely to take place.

It is interesting to compare the decomposition pathways of the naphthalenyl radicals with those for phenyl. While the energies for the H loss to produce *o*-benzyne/didehydronaphthalenes are quite similar, the ring cleavage pathways for phenyl require somewhat higher barriers than those for 1-naphthalenyl. For instance, the critical barriers to form (*Z*)-hexa-3-ene-1,5-diyne + H and *i*-C_4H_3 + C_2H_2 from phenyl were calculated[25] to be 101.7 and 99.9 kcal/mol vs. 91.9 and 97.7 kcal/mol for the analogous pathways for 1-naphthalenyl. Thus, the C-H bond β-scission is the prevailing channel of the unimolecular reaction of the phenyl radicals, whereas for the naphthalenyl radicals one can anticipate a competition between their isomerization by H migration and the H losses.

3.1.2. Acetanaphthylenyl radicals

Next, we look at isomerization and dissociation pathways of various forms of the acetanaphthylenyl radical (Figure 2). The parent molecule, acetanaphthylene, consists of two six-membered rings and a five-membered ring with two common edges with the six-membered rings and represents a prototype of a five-membered ring on a zigzag edge of PAH. Upon an H atom removal/abstraction, four different isomers of the radical can be produced, 1-, 3-, 4-, and 5-acetanaphthylenyls denoted in Fig. 2 as **an1**, **an3**, **an4**, and **an5**, respectively. Of them, **an4** is the most favorable energetically followed by **an3**, **an5**, and **an1** residing 0.2, 0.8, and 4.1 kcal/mol higher. In our analysis, we focus on the five-membered ring opening and do not consider C-H bond β-scissions since their energetic parameters and kinetics are expected to be similar to those for the naphthalenyl radical. C-C bond β-scissions in 1- and 3-acetanaphthylenyls can result in the five-membered ring cleavage. This process is relatively easier to proceed in **an1**, which can rearrange to a two ring isomer 1-ethynylnaphthalen-8-yl **an6** via a barrier of 44.8 kcal/mol. **an6** lying 29.4 kcal/mol above **an4** can further isomerize by 1,2-H migration to 1-ethynylnaphthalen-7-yl **an7** overcoming a

barrier of 59.8 kcal/mol (89.2 kcal/mol above **an4**). The **an7** intermediate is nearly isoergic with **an6**, however, it is expected to be more stable kinetically because the barrier for the reverse **an6** → **an1** isomerization is only 15.4 kcal/mol. On the contrary to **an6**, re-closure of the five-membered ring is impossible in 1-ethynylnaphthalen-7-yl **an7** but this intermediate lies on a pathway for acetylene elimination. Along this route, a 1,4-H shift in **an7** leads to **an8** via a barrier of 88.3 kcal/mol relative to **an4** and **an8** can split the C_2H_2 moiety. This process is highly unfavorable energetically and the exit transition state and the $C_{10}H_5 + C_2H_2$ product **an-p1** respectively reside 117.9 and 116.6 kcal/mol above the zero level of **an4**. The high endothermicity of this dissociation channel is related to the fact that $C_{10}H_5$ (1,2,8-tridehydronaphthalene) is a radical of an aromatic alkyne (aryne). The **an8** intermediate can be also formed directly by the C-C bond β-scission in **an3** via a transition state located 78.5 kcal/mol above **an3**.

The **an3**, **an4**, and **an5** isomers are linked by 1,2-hydrygen migrations where **an4** can rearrange to both **an3** and **an5** via barriers of 63.3 and 59.3 kcal/mol, respectively. Direct isomerization between **an1** and **an3** is hindered by a higher barrier for the 1,3-H shift, 104.6 kcal/mol relative to **an4**. Alternatively, this rearrangement can occur via a multistep pathway **an1** → **an6** → **an7** → **an8** → **an3** involving the five-membered ring cleavage, 1,2-H shift from 1-ethynylnaphthalen-7-yl to 1-ethynylnaphthalen-8-yl, 1,4-hydrogen migration, and finally, re-closure of the five-membered ring in **an8**. The highest in energy transition state along this path resides 89.2 kcal/mol above the zero level. Comparing the acetanaphthylenyl and napthalenyl PESs we can conclude that the ring cleavage pathways leading to kinetically stable products/intermediates in both cases require rather similar critical barriers to be overcome, 88-89 kcal/mol for the former vs. 92-98 kcal/mol for the latter. Whereas for naphthalenyl radicals the most likely products formed as a result of a ring cleavage are bimolecular $C_6H_4C_2H + C_2H_2$ and $C_6H_4(C_2H)_2 + H$, for acetanaphthylenyls it is the 1-ethynylnaphthalen-7-yl radical because its decomposition requires a much higher energy.

3.1.3. Pyrenyl radicals

The PES for various ring cleavage processes in the pyrenyl radical isomers, 1-, 2-, and 4-pyrenyls (**pyr1**, **pyr2**, and **pyr4**, respectively) is illustrated in Figure 3. Among the three isomers, **pyr2** has the lowest energy, with **pyr1** and **pyr4** being only slightly higher, by 0.6 and 0.2 kcal/mol, respectively. Again, here we consider only ring cleavage and isomerization pathways, while assuming that H atom losses to arynes require energies in the range of ~80 kcal/mol, similar to those for phenyl and naphthalenyl radicals. The less energy demanding ring cleavage routes involve **pyr4** and **pyr1**.

For instance, the C-C bond β-scission in **pyr4** leads to **pyr5** (4-ethynylphenanthren-5-yl) via a barrier of 55.0 kcal/mol. The intermediate **pyr5** is kinetically metastable since the barrier for the reverse ring closure to **pyr4** is only 4.6 kcal/mol. More kinetically stable 5-ethynylphenanthren-3-yl isomer **pyr6** can be produced by 1,2-hydrogen migration in **pyr5** via a barrier of 62.0 kcal/mol; the rate-determining transition state on the **pyr4** → **pyr5** → **pyr6** pathways resides at 112.6 kcal/mol relatively to the zero level of **pyr2**. **pyr6**, which lies 54.6 kcal/mol above **pyr2** can undergo acetylene desorption via a two-step mechanism involving a 1,5-H shift to **pyr7** followed by C_2H_2 elimination producing **pyr-p1** − 3,4,5-tridehydrophenanthrene, a radical which can be produced by H abstraction from phenanthryne. However, this C_2H_2 loss channel is highly endothermic with the highest in energy transition state and the product respectively lying 139.4 and 137.2 kcal/mol above **pyr2**. The intermediate **pyr7** can be also accessed directly, via the C-C bond β-scission in **pyr1** overcoming a high barrier of 100.0 kcal/mol. **pyr7** is metastable because the barriers for its rearrangements either back to **pyr1** or to **pyr6** are as low as 1.9 and 3.7 kcal/mol. Thus, two competitive ring cleavage pathways exist, **pyr4** → **pyr5** → **pyr6** and **pyr1** → **pyr7** → **pyr6** with the highest barriers of 112.6 and 101.8 kcal/mol. Another C-C bond β-scission in **pyr1** forms **pyr8** via a barrier of 69.8 kcal/mol. However, **pyr8** cannot produce any energetically favorable products and would undergo the reverse ring closure overcoming a low barrier of 3.6 kcal/mol. C-C bond β-scission in the most stable pyranyl radical isomer **pyr2** leads to **pyr9** via a 67.1 kcal/mol barrier. This metastable intermediate lies on the path to the **pyr-p2** product, phenalenyl radical + C_3 residing 137.8 kcal/mol above **pyr2**. After the initial ring cleavage, the **pyr2** → **pyr9** → **pyr10** → **pyr11** → **pyr-p2** channel involves two consecutive 1,6- and 1,2-migrations of hydrogen atoms from the side chain to aromatic rings followed by elimination of the C_3 fragment. However, this pathway is not expected to be competitive due to the unfavorable energetics and also, all three intermediates are less kinetically stable than **pyr6**, which can be formed by the ring cleavages in **pyr4** and **pyr1**.

The pyrenyl radical isomers are connected by 1,2-H and 1,3-H shifts **pyr2** ⇆ **pyr1** and **pyr4** ⇆ **pyr1** requiring barriers of 62.4 and 67.6 kcal/mol, respectively, to be overcome. These values are slightly higher than or comparable with the isomerization barrier for the naphthalenyl radical, ~60 kcal/mol, and those for the acetanaphthylenyl radicals, 59-63 kcal/mol. However, the critical barriers for the ring cleavage processes leading from the pyrenyl radicals to a relatively kinetically stable species, 5-ethynylphenanthren-3-yl **pyr6**, 102-113 kcal/mol, are clearly higher than the corresponding values for naphthalenyl and acetanaphthylenyl, 92-98 and 88-89 kcal/mol, respectively. This means that pyrenyls should be more stable with respect to the ring cleavage than their smaller counterparts.

3.2. Reaction kinetics

3.2.1. Naphthalenyl radicals

The calculated rate constants clearly demonstrate that the 1-naphthalenyl ⇆ 2-naphthalenyl isomerization is by far the fastest channel in the unimolecular reactions of **n1** and **n2**. The isomerization rate constants in both directions computed at various pressures are shown in Figure 4(a). One can see that the **n1 → n2** and **n2 → n1** rate constants are very similar to each other. The rate constants rapidly grow with temperature reaching 5.1×10^4, 1.3×10^5, 1.7×10^5, and 1.9×10^5 s^{-1} at 1500 K at the pressures of 30 Torr, 1, 10, and 100 atm, respectively. At higher temperatures, the naphthalenyl radicals eventually become unstable and equilibrate with their H loss products at the temperatures above 1800, 2000, and 2250 K at p = 30 Torr, 1 and 10 atm, respectively, but remain stable at 100 atm in the entire considered 500-2500 temperature range. Fig. 4(b) elucidates rate constants of various decomposition channels of **n1** at 1 atm compared with that for the **n1 → n2** isomerization. As anticipated for the PES analysis, the fastest dissociation channel is the H loss to **n-p3**. Still, the rate constant for this channel at 1500 K, 4.0×10^3 s^{-1}, is a factor of ~33 lower than the one for the isomerization. The rate constants at 1500 K for the H loss to **n-p4** and those for the ring cleavage channels leading to the $C_6H_4C_2H + C_2H_2$ (**n-p1**) and $C_6H_4(C_2H)_2 + H$ (**n-p2**) are further lower than the one for the H loss to **n-p3** by factors of 4.8, 7.8, and 8.0, respectively, meaning that the high temperature decomposition would predominantly occur to 1,2-didehydronaphthalene. The picture is slightly different for 2-naphthalenyl (Fig. 4(c)). Here, still the isomerization to 1-naphthalenyl is the fastest unimolecular process at all considered temperatures. The rate constants for the two H loss channels to **n-p3** and **n-p4** show relatively close values, which are factors of ~31 and 45 lower than the isomerization rate constant at 1500 K and 1 atm. The only feasible ring cleavage channels from **n2** involve its initial isomerization to **n1**, but the $n2 \to C_6H_4C_2H + C_2H_2$ (**n-p1**) and $n2 \to C_6H_4(C_2H)_2 + H$ (**n-p2**) rate constants are respectively factors of 14.8 and 16.3 lower than that for **n2 → n-p3**. The pathways of the direct ring cleavage in 2-naphthalenyl do not provide any significant contribution to its overall unimolecular kinetics; **n2** prefers to undergo a relative fast H migration to **n2** prior a ring opening can take place.

3.2.2. Acetanaphthylenyl radicals

1-acetanaphthylenyl **an1** is the least stable acetanaphthylenyl radical isomer and hence it is most prompt to the five-membered ring cleavage. Figure 5(a) illustrates rate constants for the

isomerization of **an1** to 1-ethynylnaphthalen-7-yl **an7** calculated at different pressures. The isomerization process is very slow at 1000 K but the rate constant grows higher as the temperature increases, for instance, the values at 1 atm are 1.4×10^3, 5.7×10^4, and 5.9×10^5 s^{-1} at 1500, 1750, and 2000 K, respectively. The pressure dependence is rather weak, but a slight increase of the isomerization rate constant with pressure can be seen; at 1500 K the values are 6.24×10^2, 1.37×10^3, 1.60×10^3, and 1.65×10^3 s^{-1} at 30 Torr, 1, 10, and 100 atm. The formation of the collisionally stabilized **an7** species clearly represents the most favorable isomerization/decomposition channel of **an1** up to 2000 K at 1 atm where **an7** is still kinetically stable (Fig. 5(b)), whereas at higher temperatures the isomerization **an1** → **an4** takes over. At 1500 K and 1 atm, the isomerization and decomposition routes to **an7**, **an3**, **an4**, **an5**, and **an-p1** exhibit rate constants of 1.37×10^3, 16, 11, 7, and 0.2 s^{-1} emphasizing the slow rate of these processes and the dominance of the ring cleavage of **an1** if this radical is destined to undergo a unimolecular decay. The reactions of **an7** in the reverse direction to **an1**, **an3**, **an4**, and **an5** are predicted to be two-three orders of magnitude faster, with the rate constants at 1500 K and 1 atm of 1.3×10^5, 1.7×10^4, 5.3×10^3, and 2.4×10^3 s^{-1}, respectively, whereas the decomposition of **an7** to **an-p1** has the rate constant of ~20 s^{-1}. Therefore, unimolecularly 1-ethynylnaphthalen-7-yl **an7** would preferably react back to **an1**, unless it encounters a partner for a bimolecular reaction during its lifetime, which is on a microsecond scale at this temperature, e.g., a barrierless H atom addition to form 1-ethynylnaphthalene. The equilibrium constants K_{equ}(**an1**⇆**an7**) is computed to be in the range of 0.005-0.093 in the T = 1375-2000 K temperature interval.

The other acetanaphthylenyl isomers are more likely to rearrange to one another rather than ring open to **an7**. For instance, the rate constants for **an3** → **an4** and **an3** → **an5** at 1500 K and 1 atm (see Fig. 5(d)) respectively are $\sim1\times10^5$ and 1×10^4 s^{-1}, whereas the one for **an3** → **an7** is only 49 s^{-1}, which is a factor of 28 lower than the rate constant **an1** → **an7** for the five-membered ring cleavage in 1-acetanaphthylenyl. At this temperature and pressure, the isomerization rate constants **an4** → **an3** and **an4** → **an5** (Fig. 5(e)) and **an5** → **an4** (Fig. 5(f)) are rather high, $1-2\times10^5$ s^{-1}, whereas those for their ring opening to **an7** and isomerization to **an1** are very low, 2-13 s^{-1} making these processes non-competitive. Thus, the overriding picture of the high-temperature kinetics of the acetanaphthylenyl isomers can be described as relative fast equilibration of **an3**, **an4**, and **an5**, while **an1**, if produced by H abstraction from the five-membered ring in the parent molecule, has a chance to undergo the ring cleavage. Interestingly, the overall rate constant for all ring cleavage channels in 1-naphthalenyl

in the 1375-2000 K range at 1 atm, 6.4×10^1-6.7×10^5 s^{-1}, are very close to those for the ring cleavage in 1-acetanaphthylenyl, 1.0×10^2-5.9×10^5 s^{-1}.

3.2.3. Pyrenyl radicals

For all three distinct pyrenyl isomers ring cleavage to produce the collisionally stabilized 4-ethynylphenanthren-3-yl isomer **pyr6** is very slow. For instance, the rate constants for this process at 1500 K and 1 atm are 0.8, 0.4, and 0.2 s^{-1} for **pyr1**, **pyr4**, and **pyr2**, respectively (Figure 6). The pressure dependence of these rate constants is rather weak as illustrated in Fig. 6(a) for **pyr1**. The dissociation channel to **pyr-p1** is orders of magnitude slower and hence can be neglected. Even if **pyr6** is produced, the reverse ring closure in this isomer should be fast, with the overall rate constant for the three isomerization channels to **pyr1**, **pyr4**, and **pyr2** being ~6×10^5 s^{-1} at 1500 K and 1 atm. The **pyr6** → **pyr1** rearrangement is somewhat preferred under these conditions as compared to the processes leading to **pyr4** and **pyr2** (Fig. 6(d)). In the meantime, the isomerization reactions between the three closed, four-ring pyrenyl isomers exhibit relatively large rate high-temperature rate constants. For instance, **pyr1** favors isomerization to **pyr2** over a lower barrier of 61.8 kcal/mol with the rate constant of 1.1×10^5 s^{-1} at 1500 K and 1 atm, which is more than an order of magnitude higher than the corresponding **pyr1** → **pyr4** rate constant, 8.9×10^3 s^{-1}. The reverse isomerization of **pyr2** to **pyr1** is highly preferable as compared to that to **pyr4**, with the rate constants (under the same conditions) of 8.3×10^4 and 4.7×10^2 s^{-1}, respectively. Finally, **pyr4** also tends to predominantly rearrange to **pyr1** with the rate constant of 7.3×10^3 s^{-1} as compared to 5.1×10^2 s^{-1} for **pyr4** → **pyr2**. Therefore, if we do not consider H losses to arynes, the unimolecular reaction of the pyrenyl radicals are predicted to be dominated by isomerizations between **pyr1** and **pyr2** and **pyr1** and **pyr4** via 1,2-hydrogen migrations, while the ring cleavages in these condensed PAH species are highly unlikely and much slower than those for naphtalenyl and acetanaphthylenyl radicals.

3.3. KMC simulations

The computed above radical decomposition and isomerization rate constants were tested in kinetic Monte Carlo (kMC) simulations of the PAH growth. The kMC simulations followed evolution of naphthalene in sooting-flame environments of two atmospheric burner-stabilized flames of ethylene, namely, a stagnation 16.3% C_2H_4–23.7% O_2–Ar flame of Wang and co-workers[27] (cold gas velocity 8.0 cm/s and burner-to-stagnation surface separation 0.8 cm; designated hereafter as C3H08)

and a 15.6% C_2H_2–17.7% O_2–N_2 flame of Faeth and co-workers[28] (designated XSF1.88). The flames were computed with the FFCM1 model[29] using Cantera.[30]

The stochastic evolution of PAH structure was simulated using the Gillespie algorithm[31] with an updated reaction model,[4] reproduced in Table S2 of ESI. The reaction rate constants were calculated using the time-dependent temperature and gaseous species profiles (H, H_2, C_2H_2, CH_3, O, OH, O_2) obtained in the flame simulations. The rate-constant values were updated every 10 μs. The nominal initial flame location was chosen at 1400 K and the simulations were carried out for the duration of 10 ms. Two sets of simulations were performed: 50,000 runs for flame C3H08 and 10,000 runs for flame XSF1.88.

The results of the kMC simulations are presented in Figure 7, comparing the frequencies of aromatic-ring radical cleavage and isomerization reaction events with those of major competing processes, oxidation and growth. Inspection of the middle-row panels of this figure shows that the aromatic-ring cleavage is about an order of magnitude slower than the oxyradical decomposition in the lower-sooting flame (C3H08) but the cleavage becomes comparable to the oxidation in the higher-sooting flame (XSF1.88). The latter is consistent with the earlier observation that carbon mass loss by thermal decomposition of large aromatics is comparable in rate to their mass loss by oxidation.[3] The ring-radical migration rates, displayed in the bottom panels of Figure 7, are comparable in magnitude to the rates of growth in the initial, aromatics buildup zone of both flames. The migration rate declines with the growth in aromatics size, as the aromatic edge becomes structurally more "crowded" by five-membered rings.[4]

4. Conclusions

We have explored PESs and the mechanism of an aromatic ring cleavage and isomerization for representative PAH radicals including naphthalenyl – the smallest PAH consisting of two six-membered rings, acetanaphthylenyl – a prototype of a PAH molecule with a five-membered ring on a zigzag edge, and pyrenyl – the smallest peri-fused PAH. The results indicate that a ring cleavage in naphthalenyl can produce 1-ethynylphenyl + acetylene or 1,2-diethynylbezene + H via critical barriers of ~98 and ~92 kcal/mol, respectively. The ring-cleavage channels appeared to be significantly slower than the isomerization between 1- and 2-naphthalenyl radicals via 1,2-hydrogen migration and H eliminations producing two distinct isomers of naphthyne, $C_{10}H_6$. For comparison, the ring cleavage pathways for phenyl containing only one aromatic ring exhibit higher barriers than those for naphthalenyls, ~102 kcal/mol to form (Z)-hexa-3-ene-1,5-diyne + H and ~100 kcal/mol to i-C_4H_3 +

C_2H_2.[25] For larger PAH structures, the ring cleavage is unlikely to lead to bimolecular products but can slowly produce collisionally stabilized isomers with one less ring. For instance, the cleavage of the five-membered ring in 1-acetanaphthylenyl can form 1-ethynylnaphthalen-7-yl via a critical barrier of ~84 kcal/mol and this represents the most favorable isomerization channel of **an1**. The rate constant for the ring cleavage channel beginning from **an1** appears to be comparable to the overall rate constant for the ring cleavages in naphthalenyl. However, when the radical position in acetanaphthylenyl is located on a six-membered ring (**an3-an5**), isomerizations by 1,2-H shifts are much faster than the ring cleavage. In peri-fused pyrenyl, even the ring cleavage channel without decomposition is non-competitive, as the critical barrier to produce a relatively kinetically stable isomer 5-ethynylphenanthren-3-yl rises to ~102 kcal/mol. As a result, unimolecular reactions involving pyrenyl radicals predominantly feature H-shift isomerizations. Generally, the 1,2-H shift isomerization channels have typical barriers of about 60 kcal/mol and hence are fast at high combustion temperatures. They appear to be faster than the H losses producing arynes since the *ortho* C-H bond strength in the PAH radicals is about 80 kcal/mol. Therefore, it is likely that various PAH radical isomers at high temperatures equilibrate by H migrations before they lose an H atom or undergo an aromatic ring cleavage. Moreover, the H elimination channels are likely inconsequential because the reverse aryne + H reactions are barrierless and fast. The kMC simulations show that the ring-radical migration rates are comparable with that for the PAH growth, whereas the aromatic-ring cleavage competes with the oxidation in the higher-sooting flame. The migration rate decays with the PAH size due to an increasing abundance of five-membered rings on the aromatic edges.

Conflicts of interest

There are no conflicts to declare.

Acknowledgements

Table 1. Parameters of fitted modified Arrhenius expressions $k = A\, T^n \exp(-E_a/RT)$ for the considered unimolecular isomerization and decomposition reactions calculated at 1 atm. Pre-exponential factors A are in s^{-1} and E_a are in cal mol^{-1}.[a]

Reaction	A	n	E_a	T range, K
n1 → n2	1.11E+63	-13.981	92944	1000-2000
n1 → n-p1	5.90E+86	-19.728	146980	1000-2000
n1 → n-p2	1.08E+83	-18.783	142000	1000-2000
n1 → n-p3	1.23E+51	-10.192	103870	1000-2000
n1 → n-p4	1.62E+95	-22.062	152690	1000-2000
n2 → n1	4.39E+60	-13.306	91428	1000-2000
n2 → n-p1	7.58E+116	-27.851	178560	1000-2250
n2 → n-p2	5.93E+114	-27.333	175700	1000-2250
n2 → n-p3	6.70E+64	-14.046	114130	1000-2250
n2 → n-p4	1.21E+74	-16.685	121260	1000-2250
an1 → an3	6.64E+77	-16.955	156440	1000-2000
an1 → an4	3.94E+95	-21.543	179540	1000-2500
an1 → an5	7.30E+123	-29.322	205280	1000-2000
an1 → an7	2.65E+60	-12.639	117820	1000-2000
an3 → an1	6.90E+77	-17.007	159070	1000-2000
an3 → an4	7.83E+63	-14.135	96130	1000-2000
an3 → an5	7.46E+111	-26.853	154950	1000-2000
an3 → an7	3.56E+59	-12.76	119110	1000-2000
an4 → an1	6.67E+107	-24.991	192470	1000-2500
an4 → an3	9.79E+63	-14.177	96282	1000-2000
an4 → an5	2.84E+64	-14.388	93166	1000-2000
an4 → an7	3.64E+88	-20.308	157560	1000-2000
an5 → an1	1.54E+120	-28.287	205840	1000-2000
an5 → an3	4.74E+111	-26.796	154160	1000-2000
an5 → an4	3.13E+64	-14.384	92462	1000-2000
an5 → an7	2.02E+113	-26.921	184460	1000-2000
an7 → an1	3.95E+56	-12.084	90178	1000-2000
an7 → an3	2.57E+57	-12.683	88673	1000-2000
an7 → an4	2.08E+86	-20.187	126970	1000-2000
an7 → an5	1.54E+111	-26.852	154690	1000-2000
pyr1→pyr2	5.06E+50	-10.38	87333	1000-2000
pyr1→pyr4	1.14E+37	-6.6395	82627	1000-2000
pyr1→pyr6	1.42E+50	-10.009	126850	1000-2000
pyr1→pyr-p1	4.83E+19	-0.60779	141880	1000-2000
pyr2→pyr1	5.57E+50	-10.405	87887	1000-2000
pyr2→pyr4	1.69E+89	-20.182	154360	1000-2250
pyr2→pyr6	1.19E+86	-19.312	175300	1000-2000

pyr2→pyr-p1	1.81E+58	-10.934	182930	1000-2500
pyr4→pyr1	9.22E+36	-6.6222	82943	1000-2000
pyr4→pyr2	4.28E+75	-16.359	144270	1000-2250
pyr4→pyr6	3.66E+57	-11.68	143260	1000-2000
pyr4→pyr-p1	1.23E+56	-10.089	188980	1000-2250
pyr6→pyr1	4.74E+47	-10.057	70447	1000-2000
pyr6→pyr2	6.15E+82	-19.116	117820	1000-2000
pyr6→pyr4	1.78E+56	-12.048	87295	1000-2000
pyr6→pyr-p1	5.25E+75	-17.272	128240	1000-2000

[a]The full list of calculated rate constants at different pressures can be found in ESI.

Figure Captions

Figure 1. Potential energy profile for unimolecular isomerization and decomposition of 1- and 2-naphthalenyl radicals $C_{10}H_7$. Numbers show relative energies with respect to 2-naphthalenyl **n2** in kcal/mol calculated at the G3(MP2,CC)//B3LYP/6-311G(d,p) levels of theory.

Figure 2. Potential energy profile for unimolecular isomerization and decomposition of various isomers of the acetanaphthylenyl radical $C_{12}H_7$. Numbers show relative energies with respect to 4-acetanaphthylenyl **an4** in kcal/mol calculated at the G3(MP2,CC)//B3LYP/6-311G(d,p) levels of theory.

Figure 3. Potential energy profile for unimolecular isomerization and decomposition of various isomers of the pyrenyl radical $C_{16}H_9$. Numbers show relative energies with respect to 2-pyrenyl **pyr2** in kcal/mol calculated at the G3(MP2,CC)//B3LYP/6-311G(d,p) levels of theory.

Figure 4. Rate constants for unimolecular reactions of 1- and 2-naphthaleneyl radicals: (a) **n1** → **n2** and **n2** → **n1** isomerization, dotted, solid, dashed, and dash-dotted lines show the rate constant values computed at the pressures of 30 Torr, 1, 10, and 100 atm, respectively; (b) various channels of the unimolecular reactions of 1-naphthalenyl **n1** at 1 atm; (b) various channels of the unimolecular reactions of 2-naphthalenyl **n2** at 1 atm.

Figure 5. Rate constants for unimolecular reactions of various isomers of the acetanaphthylenyl radical: (a) **an1** → **an7** – ring cleavage in 1-acetanaphthylenyl, dotted, solid, dashed, and dash-dotted lines show the rate constant values computed at the pressures of 30 Torr, 1, 10, and 100 atm, respectively; (b) various channels of the unimolecular reactions of 1-acetanaphthylenyl **an1** at 1 atm; (c) unimolecular reactions of the two-ring 1-ethynylnaphthalen-7-yl isomer **an7** at 1 atm; (d) unimolecular reactions of 3-acetanaphthylenyl **an3** at 1 atm; (e) unimolecular reactions of 4-acetanaphthylenyl **an4** at 1 atm; (f) unimolecular reactions of 5-acetanaphthylenyl **an5** at 1 atm.

Figure 6. Rate constants for unimolecular reactions of various isomers of the pyrenyl radical: (a) various channels of the unimolecular reactions of 1-pyrenyl **pyr1** at different pressures; (b) unimolecular reactions of 2-pyrenyl **pyr2** at 1 atm; (c) unimolecular reactions of 4-pyrenyl **pyr4** at 1 atm; (d) unimolecular reactions of the three-ring 4-ethynylphenanthren-3-yl isomer **pyr6** at different pressures. Dotted, solid, dashed, and dash-dotted lines show the rate constant values computed at the pressures of 30 Torr, 1, 10, and 100 atm, respectively.

Figure 7. Left panels: C3H08 flame, right panels: XSF1.88 flame; top-row panels: flame temperature; middle-row panels: rate comparison of thermal decomposition of aromatic-ring radicals with decomposition of aromatic oxiradicals; bottom-row panels: rate comparison of aromatic-ring radical

isomerization, n1 $\rightleftarrows$ n2, with the aromatic growth by C_2H_2 and CH_3 additions. The displayed frequency values are determined as the number of reaction events counted in a time interval of 0.1 ms divided by the length of the time interval and averaged over the number of kMC runs.
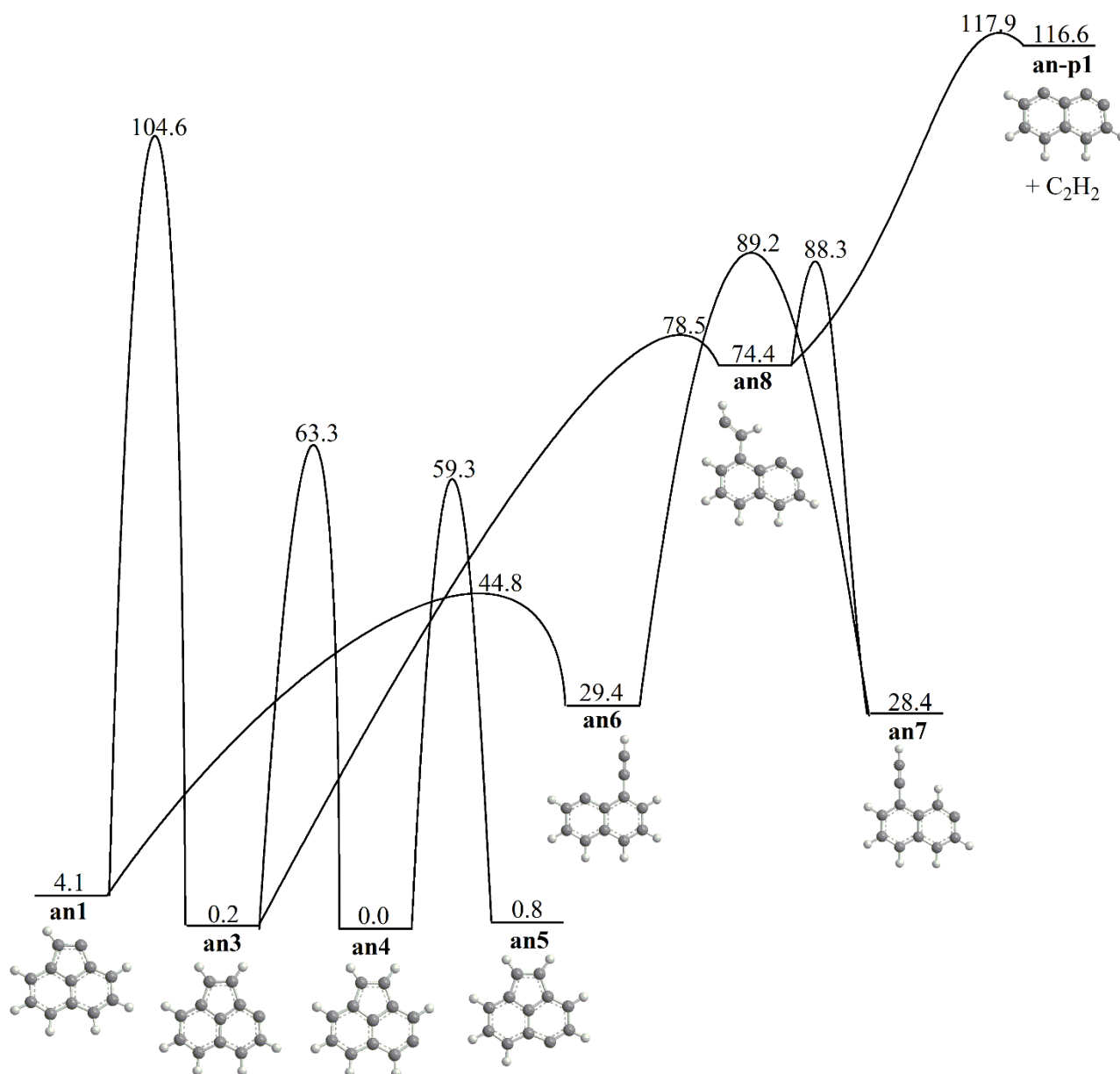
Figure 1. Potential energy profile for unimolecular isomerization and decomposition of 1- and 2-naphthalenyl radicals $C_{10}H_7$. Numbers show relative energies with respect to 2-naphthalenyl **n2** in kcal/mol calculated at the G3(MP2,CC)//B3LYP/6-311G(d,p) levels of theory.
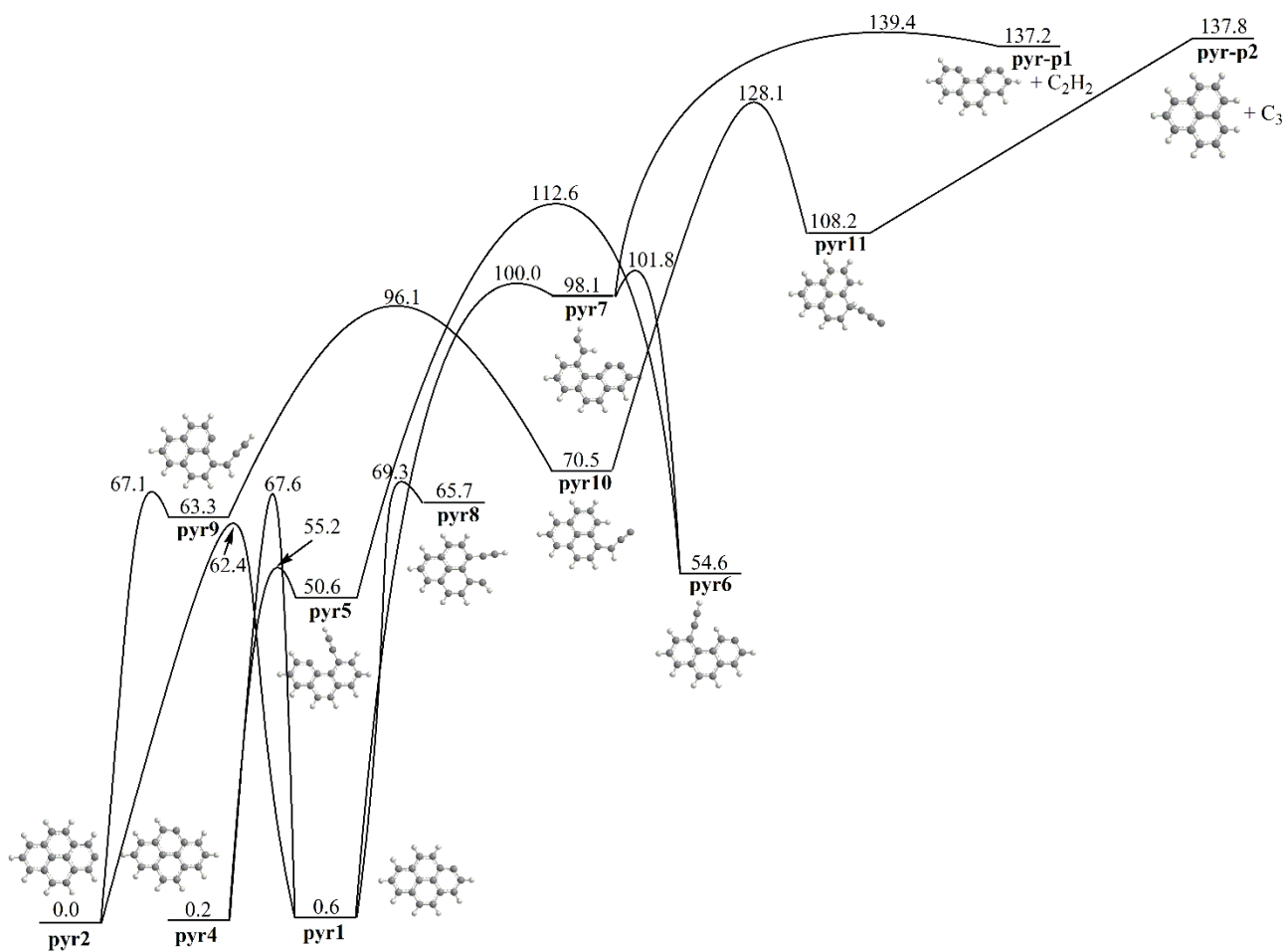
Figure 2. Potential energy profile for unimolecular isomerization and decomposition of various isomers of the acetanaphthylenyl radical $C_{12}H_7$. Numbers show relative energies with respect to 4-acetanaphthylenyl **an4** in kcal/mol calculated at the G3(MP2,CC)//B3LYP/6-311G(d,p) levels of theory.

Figure 3. Potential energy profile for unimolecular isomerization and decomposition of various isomers of the pyrenyl radical $C_{16}H_9$. Numbers show relative energies with respect to 2-pyrenyl **pyr2** in kcal/mol calculated at the G3(MP2,CC)//B3LYP/6-311G(d,p) levels of theory.
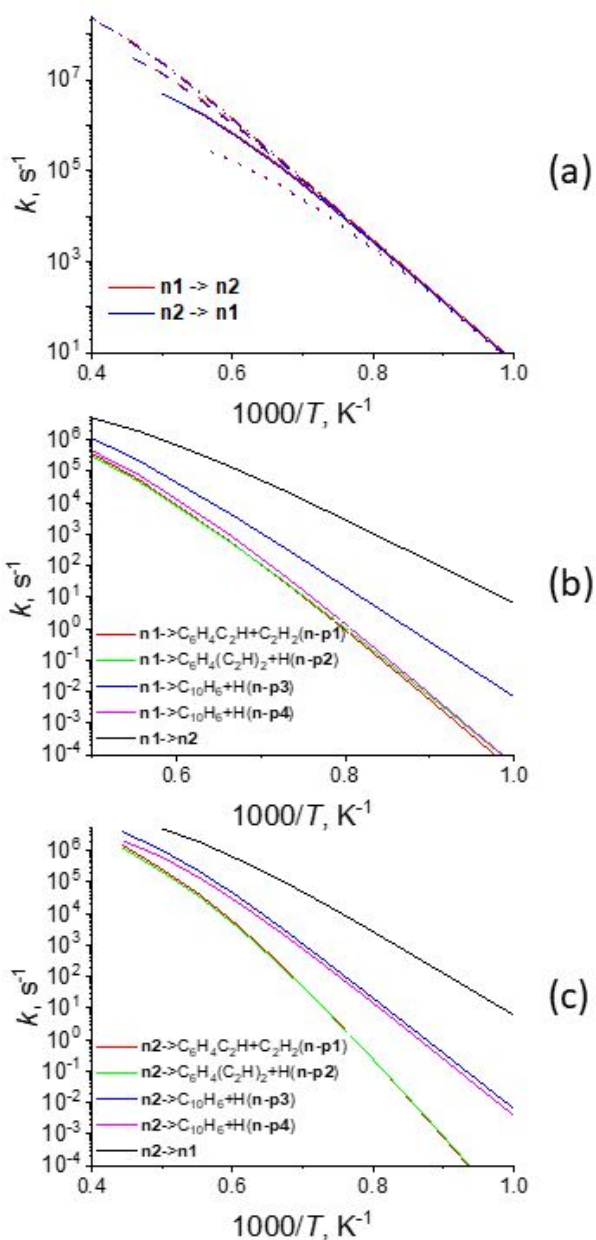
Figure 4. Rate constants for unimolecular reactions of 1- and 2-naphthalenyl radicals: (a) **n1** → **n2** and **n2** → **n1** isomerization, dotted, solid, dashed, and dash-dotted lines show the rate constant values computed at the pressures of 30 Torr, 1, 10, and 100 atm, respectively; (b) various channels of the unimolecular reactions of 1-naphthalenyl **n1** at 1 atm; (c) various channels of the unimolecular reactions of 2-naphthalenyl **n2** at 1 atm.
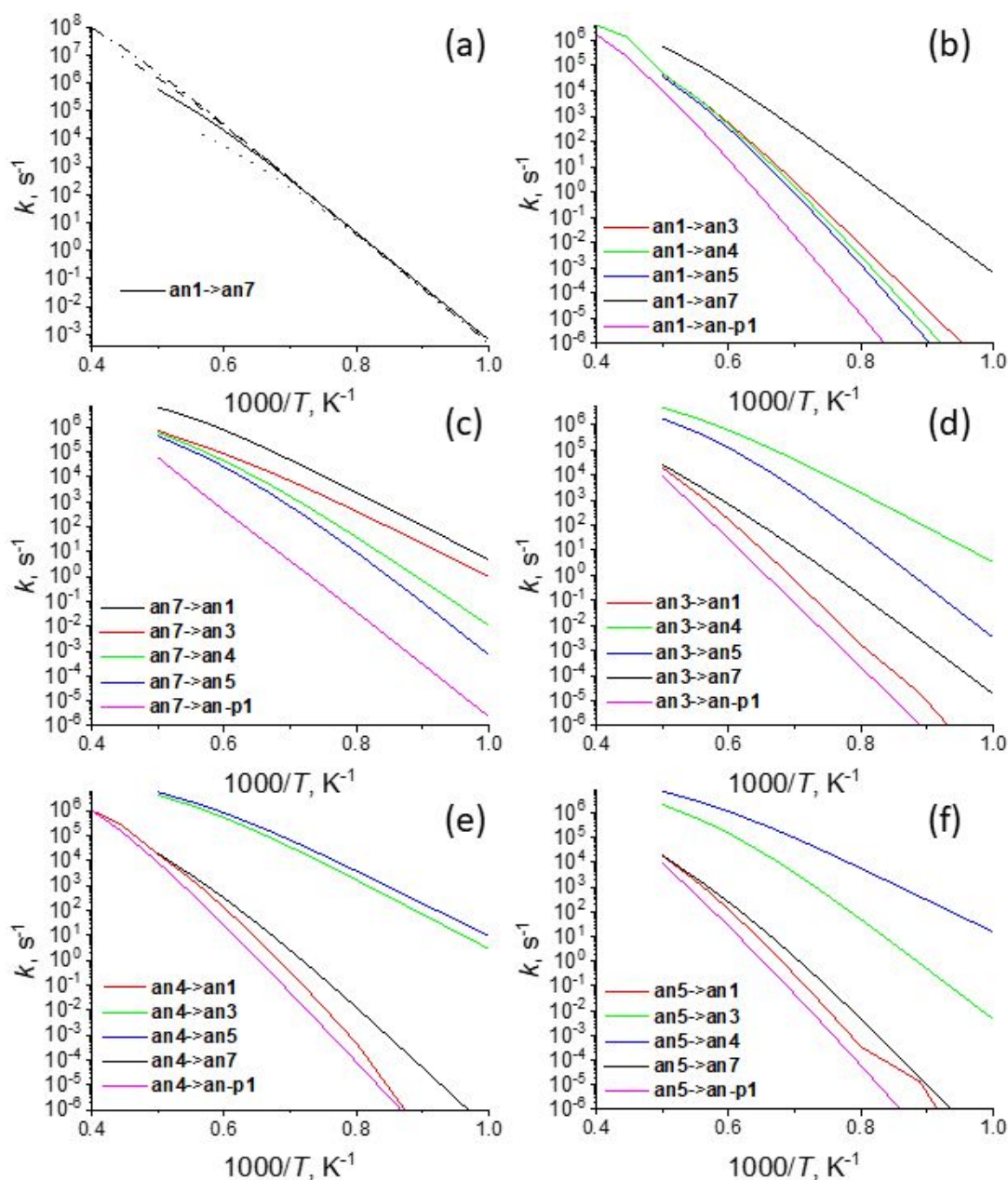
Figure 5. Rate constants for unimolecular reactions of various isomers of the acetanaphthylenyl radical: (a) **an1 → an7** – ring cleavage in 1-acetanaphthylenyl, dotted, solid, dashed, and dash-dotted lines show the rate constant values computed at the pressures of 30 Torr, 1, 10, and 100 atm, respectively; (b) various channels of the unimolecular reactions of 1-acetanaphthylenyl **an1** at 1 atm; (c) unimolecular reactions of the two-ring 1-ethynylnaphthalen-7-yl isomer **an7** at 1 atm; (d) unimolecular reactions of 3-acetanaphthylenyl **an3** at 1 atm; (e) unimolecular reactions of 4-acetanaphthylenyl **an4** at 1 atm; (f) unimolecular reactions of 5-acetanaphthylenyl **an5** at 1 atm.
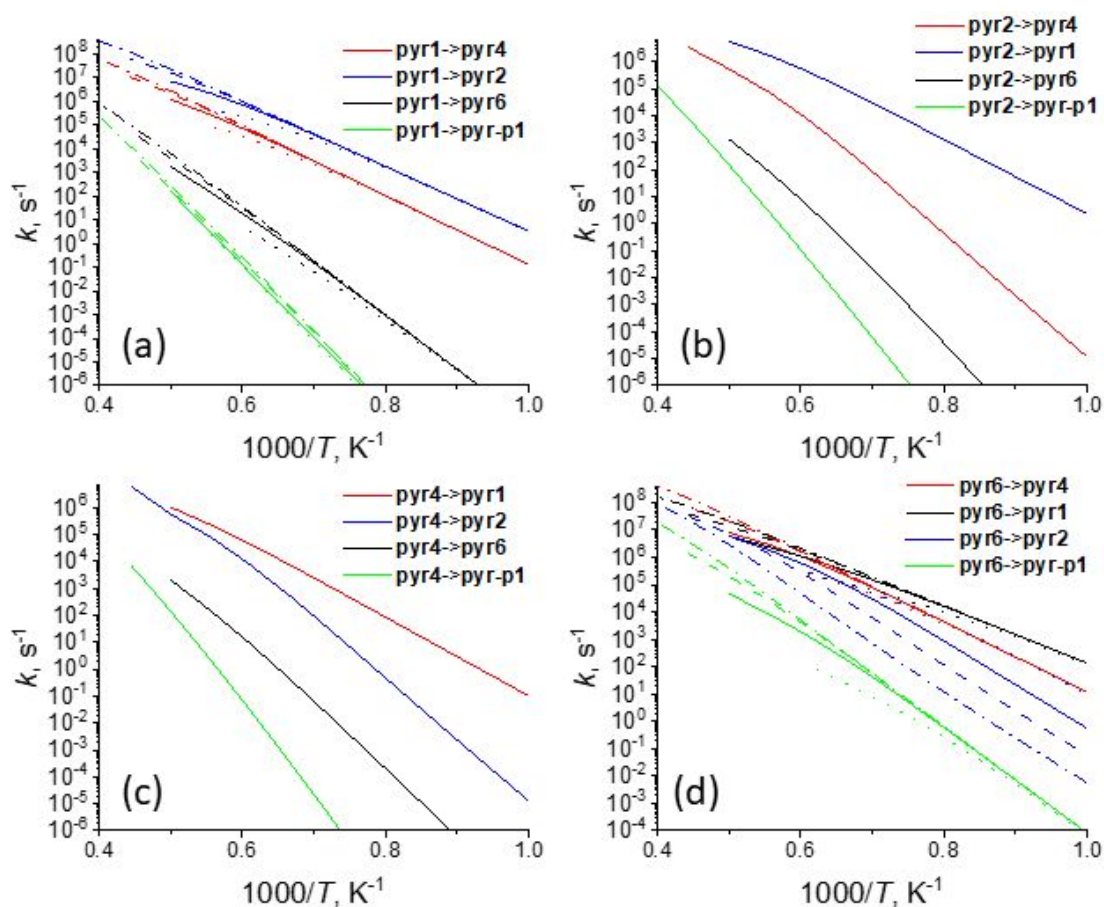
Figure 6. Rate constants for unimolecular reactions of various isomers of the pyrenyl radical: (a) various channels of the unimolecular reactions of 1-pyrenyl **pyr1** at different pressures; (b) unimolecular reactions of 2-pyrenyl **pyr2** at 1 atm; (c) unimolecular reactions of 4-pyrenyl **pyr4** at 1 atm; (d) unimolecular reactions of the three-ring 4-ethynylphenanthren-3-yl isomer **pyr6** at different pressures. Dotted, solid, dashed, and dash-dotted lines show the rate constant values computed at the pressures of 30 Torr, 1, 10, and 100 atm, respectively.
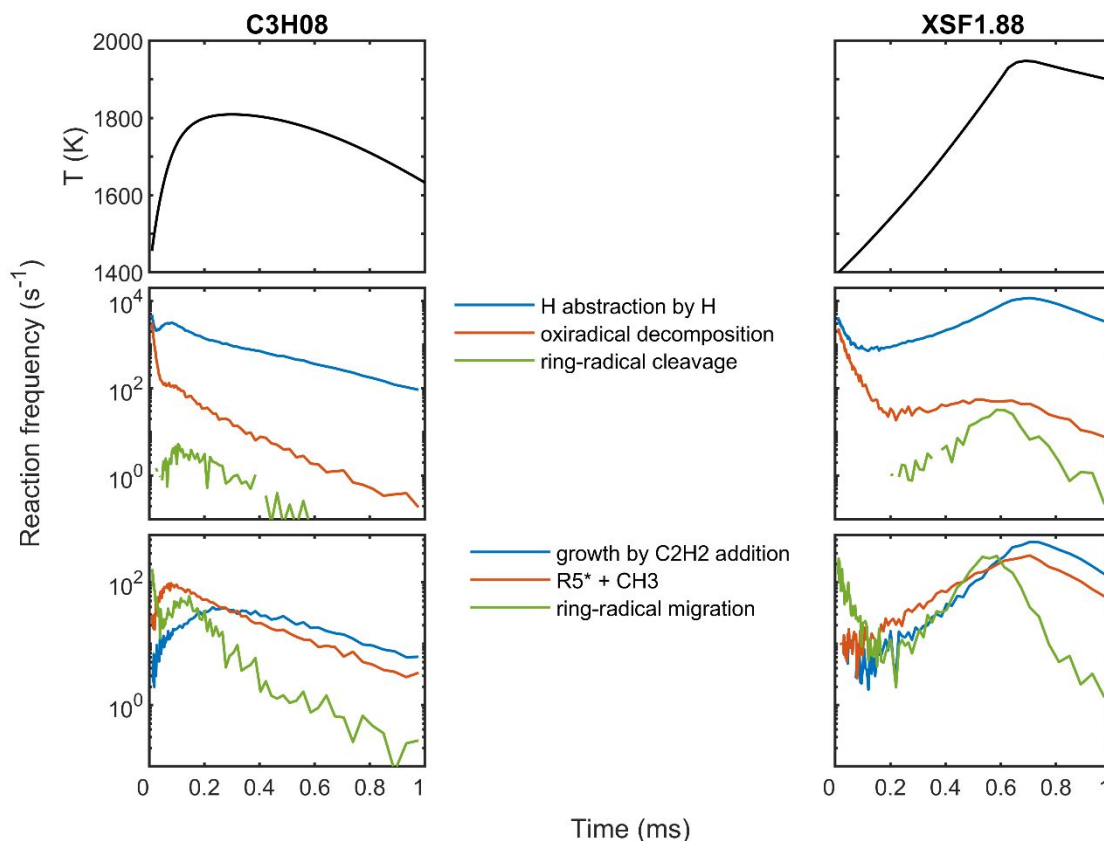
Figure 7. Left panels: C3H08 flame, right panels: XSF1.88 flame; top-row panels: flame temperature; middle-row panels: rate comparison of thermal cleavage of aromatic-ring radicals with decomposition of aromatic oxiradicals; the rate of hydrogen abstraction, the fastest reaction in the system, is also shown for comparison; bottom-row panels: rate comparison of aromatic-ring radical isomerization, n1 ⇄ n2, with the aromatic growth by C_2H_2 and CH_3 additions. The displayed frequency values are determined as the number of reaction events counted in a time interval of 0.1 ms divided by the length of the time interval and averaged over the number of kMC runs.

References

1   M. Frenklach, Reaction mechanism of soot formation in flames. *Phys. Chem. Chem. Phys.*, 2002, **4**, 2028–2037.

2   M. Frenklach and A. M. Mebel, On the mechanism of soot nucleation. *Phys. Chem. Chem. Phys.*, 2020, **22**, 5314-5331.

3   M. Frenklach, Z. Liu, R. I. Singh, G. R. Galimova, V. N. Azyazov and A. M. Mebel, Detailed, sterically-resolved modeling of soot oxidation: role of O atoms, interplay with particle nanostructure, and emergence of inner particle burning. *Combust. Flame*, 2018, **188**, 284-306.

4   M. Frenklach and A. M. Mebel, Prenucleation chemistry aromatics: A two-ring precursor? *Proc. Combust. Inst.*, **39**, submitted.

5   C. Lee, W. Yang and R. G. Parr, Development of the Colle-Salvetti correlation-energy formula into a functional of the electron density. *Phys. Rev. B: Condens. Matter Mater. Phys.*, 1988, **37**, 785−789.

6   A. D. Becke, Density-functional thermochemistry. III. The role of exact exchange. *J. Chem. Phys.*, 1993, **98**, 5648−5652.

7   M. J. Frisch, G. W. Trucks, H. B. Schlegel et al., GAUSSIAN 09, Revision A.1 Gaussian, Inc., Wallingford, CT, 2009.

8   A. G. Baboul, L. A. Curtiss, P. C. Redfern and K. Raghavachari, Gaussian-3 theory using density functional geometries and zero-point energies. *J. Chem. Phys.*, *1999*, **110**, 7650−7657.

9   L. A. Curtiss, K. Raghavachari, P. C. Redfern, A. G. Baboul and J. A. Pople, Gaussian-3 theory using coupled cluster energies. *Chem. Phys. Lett.*, 1999, **314**, 101−107.

10   L. A. Curtiss, K. Raghavachari, P. C. Redfern, V. Rassolov and J. A. Pople, Gaussian-3 (G3) theory for molecules containing first and second-row atoms. *J. Chem. Phys.*, 1998, **109**, 7764−7776.

11   MOLPRO, version 2010.1, a package of ab initio programs, H.-J. Werner, P. J. Knowles, G. Knizia, F. R. Manby, M. Schütz, and others, see http://www.molpro.net.

12   Y. Georgievskii, J. A. Miller, M. P. Burke and S. J. Klippenstein, Reformulation and solution of the master equation for multiple-well chemical reactions. *J. Phys. Chem. A*, 2013, **117**, 12146−12154.

13   Y. Georgievskii and S. J. Klippenstein, *MESS program package* 2015. https://tcg.cse.anl.gov/papr/.

14   J. Troe, Theory of thermal unimolecular reactions at low pressures. I. Solutions of the master equation. *J. Chem. Phys.*, 1977, **66**, 4745–4757.

15   A. M. Mebel, Y. Georgievskii, A. W. Jasper and S. J. Klippenstein, Temperature- and pressure-dependent rate coefficients for the HACA pathways from benzene to naphthalene. *Proc. Combust. Inst.*, 2017, **36**, 919-926.

16   H. Wang and M. Frenklach, Transport properties of polycyclic aromatic hydrocarbons for flame modeling. *Combust. Flame*, 1994, **96**, 163–170.

17   A. Vishnyakov, P. G. Debenedetti and A. V. Neimark, Statistical geometry of cavities in a metastable confined fluid. *Phys. Rev. E*, 2000, **62**, 538–544.

18   P. I. Ravikovitch, A. Vishnyakov and A. V. Neimark, Density functional theories and molecular simulations of adsorption and phase transitions in nanopores. *Phys. Rev. E*, 2001, **64**, 011602.

19   A. W. Jasper and J. A. Miller, Theoretical unimolecular kinetics for $CH_4 + M \rightleftarrows CH_3 + H + M$ in eight baths, M = He, Ne, Ar, Kr, H_2, N_2, CO, and CH_4. *J. Phys. Chem. A*, 2011, **115**, 6438–6455.

20   A. S. Semenikhin, A. S. Savchenkova, I. V. Chechet, S. G. Matveev, M. Frenklach and A. M. Mebel, Transformation of an embedded five-membered ring in polycyclic aromatic hydrocarbons via the HACA mechanism: A theoretical study. *J. Phys. Chem. A*, 2021, **125**, 3341-3354.

21   V. V. Kislov, N. I. Islamova, A. M. Kolker, S. H. Lin and A. M. Mebel, Hydrogen abstraction acetylene addition and Diels-Alder mechanisms of PAH formation: A detailed study using first principles calculations. *J. Chem. Theor. Comp.*, 2005, **1**, 908-924.

22   B. Ruscic, Active Thermochemical Tables, Version 1.122, available at http://atct.anl.gov.

23   L. V. Moskaleva, L. K. Madden and M. C. Lin, *Phys. Chem. Chem. Phys.*, 1999, **1**, 3967–3972.

24   H. Wang, A. Laskin, N. W. Moriarty and M. Frenklach, On unimolecular decomposition of phenyl radical. *Proc. Combust. Inst.*, 2000, **28**, 1545-1555.

25   A. M. Mebel and A. Landera, Product branching ratios in photodissociation of phenyl radical: A theoretical Ab initio/RRKM study. *J. Chem. Phys.*, 2012, **136**, 234305.

26   S. E. Wheeler, W. D. Allen and H. F. Schaefer, Jr., Thermochemistry of disputed soot formation intermediates C_4H_3 and C_4H_5. *J. Chem. Phys.*, 2004, **121**, 8800-8813.

27   A. D. Abid, J. Camacho, D. A. Sheen and H. Wang, Quantitative measurement of soot particle size distribution in premixed flames—The burner-stabilized stagnation flame approach, *Combust. Flame*, 2009, **156**, 1862-1870.

28   F. Xu, P. B. Sunderland and G. M. Faeth, Soot formation in laminar premixed ethylene/air flames at atmospheric pressure, *Combust. Flame*, 1997, **108**, 471-493.

29   G. P. Smith, Y. Tao and H. Wang, Foundational fuel chemistry model Version 1.0 (FFCM-1), 2016. http://nanoenergy.stanford.edu/ffcm1.

30   D. G. Goodwin, R. L. Speth, H. K. Moffat and B. W. Weber, Cantera: An object-oriented software toolkit for chemical kinetics, thermodynamics, and transport processes. https://cantera.org/. 2021.

31   D. T. Gillespie, Exact stochastic simulation of coupled chemical reactions, *J. Phys. Chem.*, 1977, **81**, 2340-2361.